## Muscle Synergy-Based Control of Human-Manipulator Interactions

Siyu Chen, Jingang Yi, and Tao Liu

Abstract—One challenge of designing robot-assisted control is to identify and estimate human intention force and motion under dynamic disturbances. We present a robotic control design to help human in manipulator-assisted upperlimb movement applications. The control design uses a muscle synergy-based neural network method to predict human force and intention motion. A disturbance observer-based controller is designed to eliminate the influence of disturbances and allows human operators to achieve task by using their normal efforts. The control design takes advantage of predicted human force and intention motion to provide proper assistance in the human-manipulator interactions. Human subject experiments are presented to demonstrate the control robustness and performance of disturbance rejection. The comparison results with a benchmark controller also confirm that the proposed design provides manipulator-assisted capability to save human effort when there are additional loads and unknown disturbances.

#### I. INTRODUCTION

The paradigm assist-as-needed design tries to help human with necessarily required assistance to finish physical tasks in many human-robot interactions applications. The amount of needed assistance is commonly calculated as the capability gap between that needs to achieve the required task and human intention or capability [1]. Additionally, robotic assistance should also be robust to the changing environment and external disturbances. The motivation of this work lies in many applications in which robotic manipulators would augment human capability (e.g., strength and accuracy) as well as disturbance rejection. One of direct applications is the robot-assisted grit-blasting process, in which human operators provide guidance to the manipulator to conduct forceful grit-blasting task, while the process generates a large reactive disturbance force to the human-robot interface [2]. Under the robot assistance, the human operators would ideally apply their nominal forces (e.g., voluntary movement) to guide the robot without significant influence by the reactive process disturbance force. The goal of this paper is to present a human muscle synergy model-based assist-asneeded manipulator control for human-robot interactions in the above-mentioned blasting process.

Muscle synergy model was an enabling tool for human effort estimation [3], [4]. Muscle synergy represents a group of relationship-fixed muscle activities during a particular

This work was supported in part by the US National Science Foundation under award CMMI-1762556.

human limb motion [5]. Human limb motion and its forceful interactions with environment can be captured as a set of muscle synergy combination. For example, using four muscle synergies, approximately 90% of all muscle activities and variability can be reconstructed during a postual task [6]. Electromyography (EMG) measurements are commonly used to construct muscle synergies [5]. However, it is not convenient to wear EMG probes in many human-robot interactions to monitor and obtain muscle activation in practical applications. We take advantages of muscle synergy model and estimate human forces without using EMG sensors.

To achieve a proper assistance in human-manipulator interaction tasks, it is desirable to obtain human force and intention motion. Neural networks method is particularly suitable for human intention motion estimation because of its capability to handle highly uncertain, nonlinear and complex systems [7], [8]. Combining with the muscle synergy models, the neural network design can accurately predict the human-robot interaction forces. One rationale for this design is the feasibility to use a same set of muscle synergies to model human arm motion and endpoint force [9].

Impedance control [10] and learning control [11] are usually considered for physical human-robot interactions. Gribovskaya *et al.* construct a learning task model to generate reference kinematic signals [12]. To reject known disturbances, a combined feedforward and compensatory control was designed in [13] to achieve pursuit tracking. Disturbance-rejection ability is critical for many human-robot interactions, such as robot-assisted grit-blasting process aforementioned, in which disturbance reaction force can be large enough to hurt human operators if the manipulator does not share these forces completely or partially. Moreover, individual persons have distinctive muscle strength capacities and thus, the robot control needs to be robust to deal with these variations.

In this paper, we develop a muscle synergy-based force control of human-manipulator interactions. Using the muscle synergy models, supervised neural networks are used to predict the human force and intention motion trajectory without use of EMG device. Under the proposed control, the robot follows human intention motion and provide necessary assistance to compensate for external load and unknown disturbances. The control performance is demonstrated through multi-subject experiments. The main contribution of the work lies in the muscle synergy-based robotic control for disturbance rejection and human effort assistance.

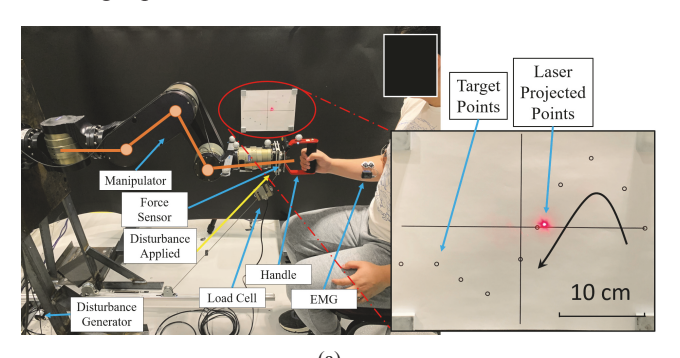
S. Chen and J. Yi are with the Department of Mechanical and Aerospace Engineering, Rutgers University, Piscataway, NJ 08854 USA (e-mail: siyu.chen@rutgers.edu; jgyi@rutgers.edu).

T. Liu is with the State Key Lab of Fluid Power and Mechatronic Systems and the School of Mechanical Engineering, Zhejiang University, Hangzhou, Zhejiang 310027, China (email: liutao@zju.edu.cn).

# II. MUSCLE SYNERGY-BASED HUMAN FORCE AND INTENTION MOTION ESTIMATION

#### A. Synergy-Based Human Force Model

Fig. 1(a) shows an example of manipulator-assisted human material handling applications. Fig. 1(b) illustrates the modeling schematic for the arm-manipulator interactions. For simplicity, the motion of manipulator end-effector O is under guidance of human operator in the vertical plane, that is, the XZ-plane in Fig. 1(b). Human operator is assumed to only knows a set of target points (not entire trajectory), with positions denoted as  $r^d$ . Human operators plan the trajectory and try to use voluntary motion to guide the robot to pass these target points.



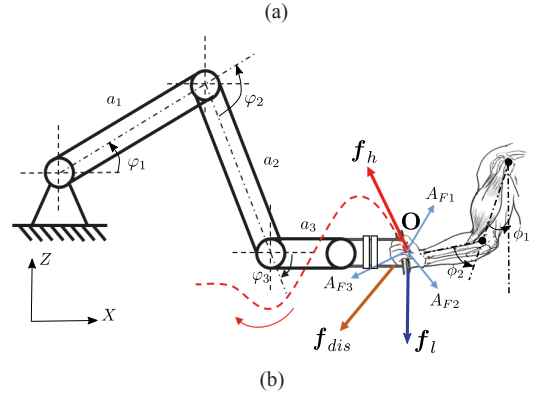


Fig. 1. (a) Human-manipulator interactions experiment setup. The right zoom-in picture shows the set of target points to follow and current end-effector position (in the vertical plane) indicated by a laser pointer. (b) The schematic of the human upper-limb model and its interaction with a robotic manipulator in the planar motion.

To design an assist-as-needed strategy, it is critical to estimate human applied forces and motion and muscle synergy is used as a modeling tool. Muscle force  $f_h$  at a joint can be expressed as a function of arm posture as [14]

$$f_h = a(t)F^{\max} f_l(q_h) f_v(\dot{q_h}) \cos \alpha, \tag{1}$$

where  $q_h$  represents the joint angle, a(t) is a muscle activation factor,  $F^{\max}$  is the maximum force that can be generated from the muscle. Functions  $f_l(q_h)$  and  $f_v(\dot{q}_h)$  capture the force-length and force-velocity relationships, respectively. Variable  $\alpha$  is the pennation angle and is assumed constant.

Muscle synergy represents a group muscles that activate together at a relative fixed activation ratio. From modeling and control purposes, muscle synergy provides a lowdimensional representation of muscle activities for human movement. Upper-limb motion is driven by multiple muscles and synergies and the muscle activation is expressed as a linear summation of spatial and temporal patterns of muscle synergies as [15]

$$M(q_h, t) = \sum_{i=1}^{n} c_i(t) w_i = W(q_h) C(t), \qquad (2)$$

where  $q_h$  is the arm joint angle vector (e.g., elbow and shoulder angles).  $M(q_h,t) \in \mathbb{R}^N$  is the muscle activation vector at time t and  $q_h$ , N is the number of muscles,  $W(q_h) = [w_1 \cdots w_n] \in \mathbb{R}^{N \times n}$  is the spatial pattern of the muscle synergy matrix, n is the number of muscle synergies, and  $C^T(t) = [c_1(t) \cdots c_n(t)]^T \in \mathbb{R}^n$  is temporal pattern vector of the muscle synergy.  $w_i$  and  $c_i(t)$  denote the ith muscle synergy and activation level, respectively.

For voluntary movement, we used an optimization method to explain the observation that solution of minimizing  $\Delta E_h$  would result in a synergy model. Within time duration  $\Delta T$ , human effort  $\Delta E_h$  is estimated as [16]

$$\Delta E_h = \frac{1}{\Delta T} \int_0^{\Delta T} E_h(t) dt = \frac{1}{\Delta T} \int_0^{\Delta T} \sum_{j=1}^{n_\tau} M_j^2(t) dt,$$
(3)

where  $E_h(t) = \sum_{j=1}^{n_\tau} M_j^2(t)$ ,  $M_j > 0$  is the jth element of muscle activation vector  $\boldsymbol{M}(\boldsymbol{q}_h,t)$ .

From [3], human force at end-effector O is written as

$$\boldsymbol{f}_h(\boldsymbol{q}_h, \dot{\boldsymbol{q}}_h) = \boldsymbol{A}_F(\boldsymbol{q}_h, \dot{\boldsymbol{q}}_h)\boldsymbol{C}(t), \tag{4}$$

where  $A_F(q_h, \dot{q}_h) \in \mathbb{R}^{3 \times n}$  is the gain matrix that depends on muscle force model (1) and Jacobian matrix from the joint rates to the endpoint velocity of O. We use human nominal force measurements  $f_h$  and synergy activation C(t) that was obtained from EMG measurements to estimate the value of  $A_F(q_h, \dot{q}_h)$  off-line by regression method (e.g., least-square) and then use (4) to compute human force in real time. To estimate the value of  $A_F(q_h, \dot{q}_h)$ , we take multiple subjects data that cover the variance of synergy model.

#### B. Human Force and Intention Motion Estimation

To estimate the human force by (4), we need to predict human neuro-control activation level C(t). For planar movement, we construct a relationship between synergy activation and tracking error as  $C(t) = C(\Delta q_h, \Delta \dot{q}_h, \Delta \ddot{q}_h)$ , where  $\Delta q_h(t) = q_h(t) - q_h^d(t)$ ,  $q_h^d(t) = \mathrm{inv}(r_r(t))$  is the human arm joint angle profile for intention trajectory  $r_r(t)$  in Cartesian space (i.e., working space), and  $\mathrm{inv}(\cdot)$  is the inverse kinematic mapping of the two-link human arm. We use a neural network approach to estimate muscle activation level C(t) in real time. Radial basis function neural networks are considered to obtain the predictions. The prediction output  $\phi(\Lambda, \nu)$  of neural networks is expressed as

$$\phi(\mathbf{\Lambda}, \mathbf{\nu}) = \mathbf{\Lambda}^T \mathbf{S}(\mathbf{\nu}), \tag{5}$$

where  $S(\nu) = [s_1(\nu) \cdots s_p(\nu)]^T$ ,  $s_k(\nu) = \exp\left[\frac{-(\nu-\mu_k)^T(\nu-\mu_k)}{\eta_k^2}\right]$  is the base function,  $k=1,\ldots,p,p$  is the total number of base functions,  $\nu$  is the input of the

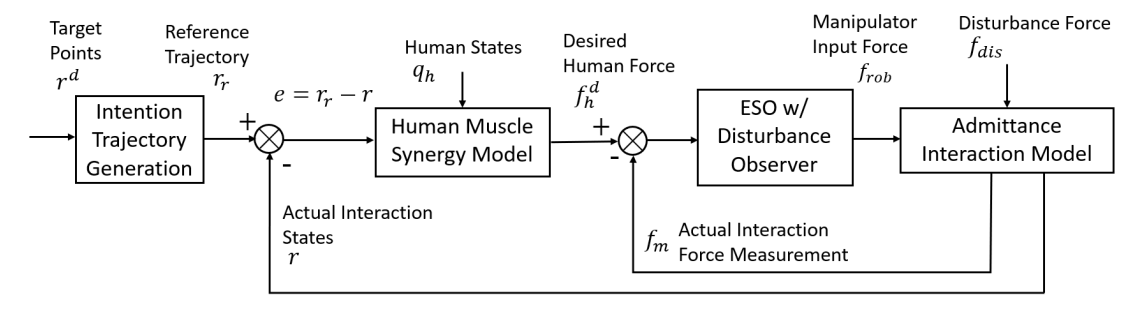


Fig. 2. Schematic of the human-robot interactions control design.

neural network,  $\mathbf{\Lambda}$  is an adjustable weight vector, and  $\boldsymbol{\mu}_k$  and  $\eta_k$  are constant parameters. To estimate  $\boldsymbol{C}(t)$  by (5), the inputs of the neural networks is  $\boldsymbol{\nu}_C = [\Delta \boldsymbol{q}_h \ \Delta \dot{\boldsymbol{q}}_h \ \Delta \ddot{\boldsymbol{q}}_h \ q_h^d]^T$ ,  $i=1,\ldots,L_f,L_f$  is the size of training data set for intention force estimation, and  $\boldsymbol{q}_h^d$  is the targeted arm motion profile.

Human operators only know to reach a set of target points  $r^d$ , not the entire desired trajectory  $r_r$ . Therefore, we use and extend the approach in [17]. Human intention motion  $r_r$  is estimated by the interaction force  $f_h$ , actual end-effector position r and velocity  $\dot{r}$  and (discrete) target points  $r^d$ . We take  $\nu_r = [f_{hi}^T r_i^T \dot{r}_i^T r_i^d]^T$ ,  $i = 1, \ldots, L_r$ ,  $L_r$  is the size of training data set. The training process is conducted off-line and the intention predictions are implemented in real time.

#### III. HUMAN-ROBOT INTERACTION CONTROL

The robotic manipulator is considered by a three-link rigid body and the dynamics model is expressed as [18]

$$\boldsymbol{M}_{r}\ddot{\boldsymbol{q}} + \boldsymbol{D}_{r}\dot{\boldsymbol{q}} + \boldsymbol{G}_{r} = \boldsymbol{J}^{T}\left(\boldsymbol{f}_{h} + \boldsymbol{f}_{l} + \boldsymbol{f}_{dis}\right) + \boldsymbol{\tau}_{rob}, \quad (6)$$

where  $q = [\varphi_1 \ \varphi_2 \ \varphi_3]^T$  is the joint angle vector,  $M_r$ ,  $D_r$ , and  $G_r$  are the manipulator's inertia, Coriolis, and gravity matrices, respectively. Due to page limit, we omit details of these matrices here. In (6),  $f_h$  is the human applied force,  $f_l$  is the known load,  $f_{dis}$  is the unknown disturbance force, and  $\tau_{rob}$  is the robot input torque vector of the fully-actuated manipulator. J is the Jacobian matrix between the end-effector velocity  $\dot{r}$  and joint rate  $\dot{q}$ .

Considering  $\dot{r} = J\dot{q}$  and  $\ddot{r} = JJ^{-1}\dot{r} + J\ddot{q}$ , we rewrite (6) into the end-effector motion as

$$M\ddot{r} + D\dot{r} + G = f_{ext} + f_{dis} + f_{rob}, \tag{7}$$

where  $\boldsymbol{f}_{ext} = \boldsymbol{f}_h + \boldsymbol{f}_l, \ \boldsymbol{f}_{rob} = \boldsymbol{J}^{-T}\boldsymbol{\tau}_{rob}, \ \boldsymbol{M} = \boldsymbol{J}^{-T}\boldsymbol{M}_r\boldsymbol{J}^{-1}, \ \boldsymbol{D} = \boldsymbol{J}^{-T}(\boldsymbol{D}_r - \boldsymbol{M}_r\boldsymbol{J}^{-1}\dot{\boldsymbol{J}})\boldsymbol{J}^{-1}, \ \text{and} \ \boldsymbol{G} = \boldsymbol{J}^{-T}\boldsymbol{G}_r.$  Note that human force  $\boldsymbol{f}_h$  is estimated using (4). The force sensor mounted at the end-effector directly obtains the measurement of total force  $\boldsymbol{f}_m = \boldsymbol{f}_{ext} + \boldsymbol{f}_{dis}$ .

the measurement of total force  $\boldsymbol{f}_m = \boldsymbol{f}_{ext} + \boldsymbol{f}_{dis}$ . The control goal is to generate a desired admittance model between external force  $\boldsymbol{f}_{ext}$  and the end-effector position  $\boldsymbol{r}$  [19]. Under known force  $\boldsymbol{f}_{ext}$  and a desired admittance model, the end-effector motion is obtained by

$$M_d\ddot{r} + D_d\dot{r} + K_dr = f_{ext}, \tag{8}$$

where  $M_d$ ,  $D_d$ ,  $K_d \in \mathbb{R}^{3\times 3}$  are (symmetric and positive definite) desired inertia, damping, and stiffness matrices, respectively. When robot dynamics (7) is known, the control

input u is designed as  $u = f_{rob} = -\hat{f}_h + M\ddot{r} + D\dot{r} + G - v$ , where  $\hat{f}_h$  is the estimate of force  $f_h$  by the synergy-based model and v is the auxiliary control input that will be designed later in this section. Plugging into (7) and (8), we have

$$M_d\ddot{r} + D_d\dot{r} + K_dr = \hat{f}_h + v - f_{dis}. \tag{9}$$

The human-robot interaction should have the desired admittance between the desired human force  $f_h^d$  and the reference motion  $r_r$ , namely,  $M_d\ddot{r}_r + D_d\dot{r}_r + K_dr_r = f_h^d$ , where  $f_h^d$  is desired human force and  $r_r$  is the end-effector position reference. Defining error  $e = r_r - r$  and using (9) and the above equation, we obtain

$$oldsymbol{f}_{dis} = \hat{oldsymbol{f}}_h - oldsymbol{f}_h^d + (oldsymbol{M}_d \ddot{oldsymbol{e}} + oldsymbol{D}_d \dot{oldsymbol{e}} + oldsymbol{K}_d oldsymbol{e}) + oldsymbol{v} = oldsymbol{g} + oldsymbol{B} oldsymbol{v},$$

$$(10)$$

where  $\boldsymbol{B} = \boldsymbol{I}_3$  and

$$g = \hat{f}_h - f_h^d + (M_d \ddot{e} + D_d \dot{e} + K_d e).$$
 (11)

We design a manipulator controller to assist human achieving desired interaction admittance along the trajectory and reject disturbances. Fig. 2 illustrates the control design structure. The controller is built on an extended state observer (ESO) to maintain the human desired force and reject the disturbance. To design an ESO, we first introduce state variables  $\dot{x}_1 = f_{dis} \in \mathbb{R}^3$ ,  $x_2 = g \in \mathbb{R}^3$ , and then write (10) into an extended state space form

$$\dot{x}_1 = x_2 + Bv, \ \dot{x}_2 = \dot{g}, \ y = x_2,$$
 (12)

Using (12), an ESO is constructed as follows.

$$\dot{z} = \begin{bmatrix} 0 & I_3 \\ 0 & 0 \end{bmatrix} z + \begin{bmatrix} B \\ 0 \end{bmatrix} v + L(y - \hat{y}), \ \hat{y} = z_2, \quad (13)$$

where  $\mathbf{z} = [\mathbf{z}_1^T \ \mathbf{z}_2^T]^T \in \mathbb{R}^6$  is the estimate vector of  $\mathbf{x} = [\mathbf{x}_1^T \ \mathbf{x}_2^T]^T$ ,  $\hat{\mathbf{y}}$  is the estimate of  $\mathbf{y}(t)$  by using  $\mathbf{z}$  and  $\mathbf{L} = [\mathbf{L}_l \otimes \mathbf{I}_3]$  is the observer gain vector,  $\mathbf{L}_l = [\mathbf{l} \ \mathbf{l}]$ ,  $\mathbf{l} = [l_1 \ l_2]^T$ ,  $\otimes$  represents the Kronecker product, and  $\mathbf{I}_n$  represents the  $n \times n$  identity matrix. The values of  $l_1$  and  $l_2$  are chosen such that the observer poles are placed at  $-\omega_0$  ( $\omega_0 > 0$ ), namely,  $s^2 + l_1 s + l_2 = (s + \omega_0)^2$ .

With the proper ESO design, the estimate of z converges to an neighborhood of x if  $\|\dot{g}\|$  is small. A proportional-derivative (PD) control structure is designed for the auxiliary input v to drive z to zero, namely,

$$v = k_p(-z_1) + k_d(-z_2),$$
 (14)

where  $k_p$  and  $k_d$  are the positive gain matrices. The stability of the controller design is obtained through the separation principle of the linear systems for (13) under the approximation  $\dot{g} \approx 0$ . If  $\dot{x}_2 = \dot{g}$  is bounded around 0 uniformly, we can show that  $\|z - x\|$  and  $\|z_2\|$  is bounded around zero closely as  $t \to \infty$ . Then  $\|\hat{f}_h - f_h^d + (M_d\ddot{e} + D_d\dot{e} + K_de)\|$  is bounded around zero, and thus, accordingly both force  $\|\hat{f}_h - f_h^d\|$  and position  $\|e\|$  are bounded around zero. We omit the detailed convergence proof due to page limit.

#### IV. EXPERIMENTS AND RESULTS

Ten subjects were recruited for experiments (nine male and one female, age:  $28.4 \pm 2.5$  years, height:  $172.1 \pm 4.4$ cm, weight:  $71.3 \pm 7.3$  kg). The subjects were identified as healthy and capable to hold and move objects using upper-limbs. Fig. 1(a) shows the human upper-limb interactions with a 3-DOF manipulator (from Schunk GmhH & Co, Germany). In experiment, the subjects were trained to operate the manipulator by grasping the handle at the end-effector. The subject's hand can move freely with the end-effector handle and the manipulator was run under a compliance controller, denoted as benchmark controller, which is described in [20]. Under the benchmark control, the robotic manipulator follows human intention motion trajectory with a desired admittance. An informed consent form was signed by all the subjects and the testing protocol was approved by the Institutional Review Board (IRB) at Rutgers University.

The upper-limb movements were obtained by the motion capture system at sampling frequency of 100 Hz (7 Bonita cameras, Vicon, Inc., Oxford Metrics, Oxford, UK). The human-robot interaction force was measured by a 6-DOF force sensor (sample rate of 1000 Hz; model Mini45 from ATI Inc.) mounted at the end-effector. The disturbance force was generated from a motor pulling a steel cable in both horizontal and vertical directions. The disturbance force was measured by a load cell (Model XTS4: S-Type from Load Cell Central) at a sampling frequency of 200 Hz. Both the benchmark and proposed controllers were implemented and running at 200 Hz. To estimate muscle synergies, a surface EMG system (MyoMuscle, Noraxon Inc.) was used to measure the muscle activities and sampling rate of EMG system was 1500 Hz. Eight muscle activities are measured, including Brachialis (BRD), Biceps (BI), Medial triceps (MTRI), Lateral triceps (LTRI), Anterior deltoid (ADELT), Medial deltoid (MDELT), Posterior deltoid (PDELT), and Pectoralis major (PECT).

The main goal for conducting experiments is to validate and demonstrate the feasibility of the proposed modeling and control systems design. The human subjects were instructed to guide the robotic end-effector in planar motion in the vertical plane. In experiments, the subjects moved the end-effector to pass a set of target points (i.e., discrete points) using their preferred motion and trajectory and they were not asked to enforce precisely motion strictly. The manipulator passively follows human intention to reach the target

points. The actual end-effector trajectory was shown on a computer monitor and its actual position was also physically projected on a nearby paperboard by using a laser pointer; see Fig. 1(a). The subjects repeated the exact same task for multiple times in experiments and they also practiced several times before actual experiment.

Disturbances were introduced and applied to the endeffector at random time in experiments. Under disturbances, two sets of experiments were conducted: human subjects tried to correct and overcome disturbance forces under the benchmark controller and the proposed controller. Each type of experiments was repeated for three trials and subjects took a brief rest (5-10 mins) between each trial. Before each trial, the subject was asked whether they feel tired or if they need additional rest to start the experiments.

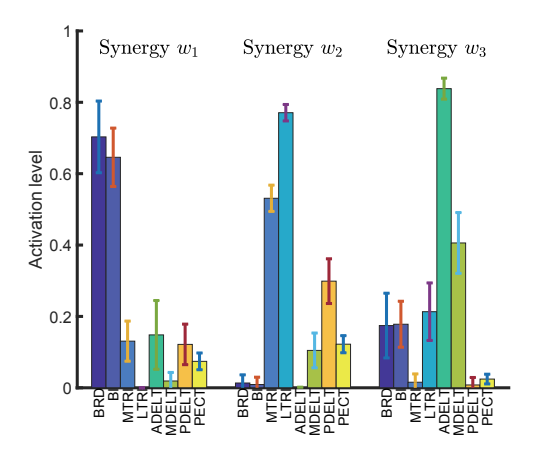


Fig. 3. Human upper-limb synergies ( $w_1$ ,  $w_2$  and  $w_3$ ) obtained from upper-limb movement in planar motion of the end-effector. Each synergy contains eight muscles: BRD, BI, MTRI, LTRI, ADELT, MDELT, PDELT, and PECT. The muscle activation variances of each synergy pattern are calculated from multi-subjects tests.

Three synergies are selected for human upper-limb motion. We chose three synergies because they can reliably reproduce more than 90% of EMG activities [6] and therefore can capture arm muscle activities in planar motion in experiments. Fig. 3 shows the synergy patterns (i.e., denoted as  $w_1$ ,  $w_2$ , and  $w_3$ ) as a histogram and the variances of each muscle activation level are shown as vertical bars. These synergy patterns are obtained by measuring all subjects experiments.

 $\label{table I} \mbox{ROOT MEAN SQUARE (RMS) ERRORS FOR VARIOUS PREDICTIONS}$ 

NN predicted force (N)		Reconstructed force (N)		Predicted traj (mm)	
X-direction	Z-direction	X-direction	Z-direction	X-direction	Z-direction
$3.2 \pm 0.4$	$3.7 \pm 0.3$	$5.1 \pm 1.4$	$5.6 \pm 1.4$	$3.0 \pm 1.1$	$2.9 \pm 0.5$

With the synergy-based force and intention prediction, Fig. 4 demonstrates the control performance under external disturbance force. For comparison purpose, we also include the results under the benchmark controller, under which the robot follows human motion passively with a desired admittance. Fig. 4(a) shows the end-effector trajectory profiles along the X- and Z-direction. In the figure, four curves

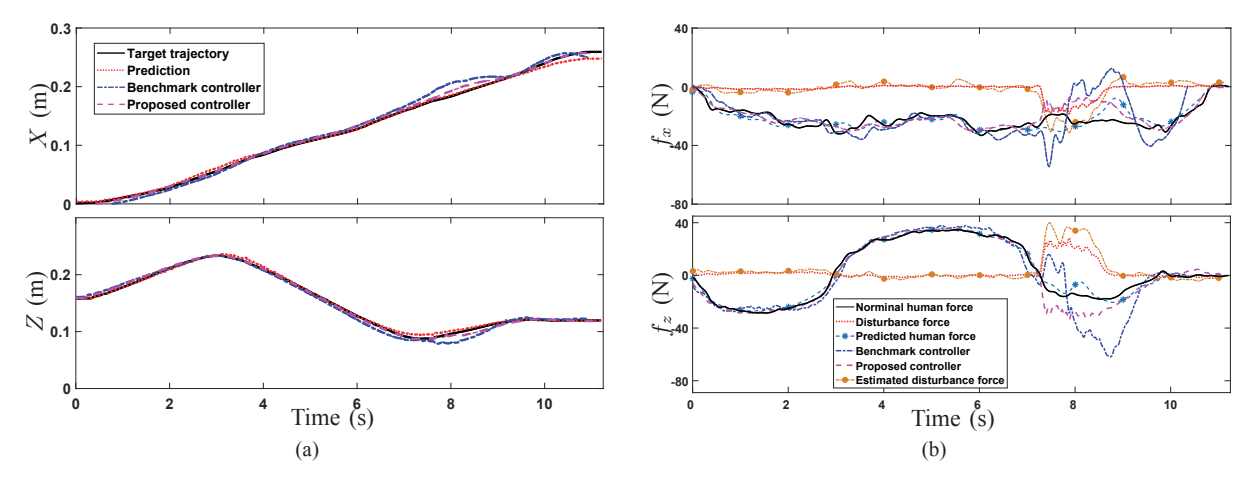


Fig. 4. Experimental results under disturbance force by one subject. (a) End-effector motion trajectory. The top plot shows the trajectory in the X-direction and the bottom for the Z-direction. (b) Human and disturbance forces profiles at the end-effector. The top plot shows the force  $f_z$  along the X-direction and the bottom  $f_z$  for the Z-direction.

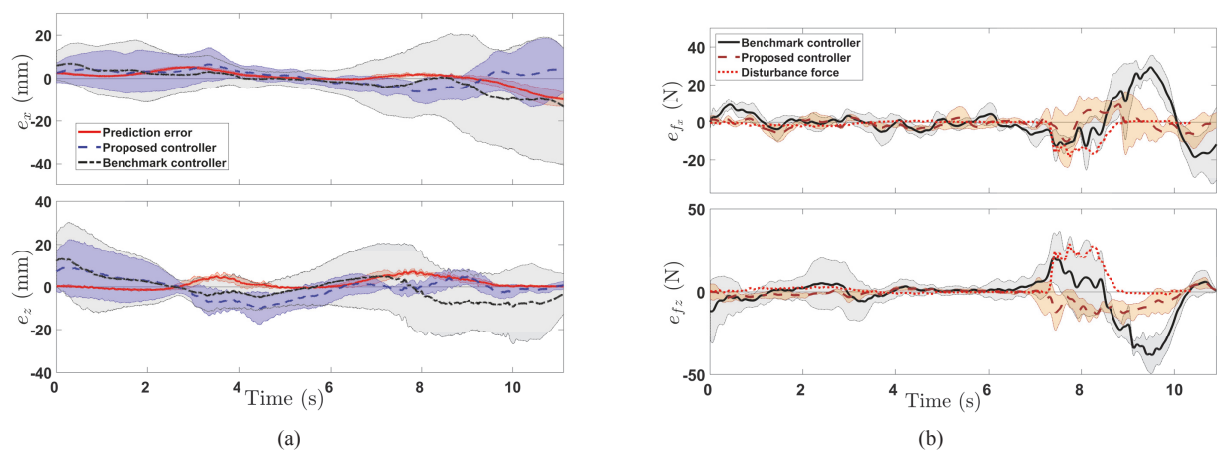


Fig. 5. (a) End-effector motion trajectory error profiles comparison for all ten subjects. The top figure shows the X-direction position error  $\mathfrak{E}$  and the bottom for Z-direction position error profile  $e_z$ . The thick curves are the mean value profiles and the shaded areas show the one standard deviation around the mean values of all subject experiments. (b) Human force error profiles comparison for all ten subjects. The top figure shows the X-direction force error  $e_{fx}$  and the bottom for Z-direction force error profile  $e_{fz}$ .

are plotted: nominal trajectory (black solid curves), neural network-based human intention motion trajectory (red dotted curves), actual trajectories under the benchmark (blue dashdotted curves) and the proposed controllers (magenta dash curves). Fig. 4(b) shows the corresponding human forces comparison in experiments.

Fig. 5(a) further shows the statistics of the position errors of all ten subjects (using the nominal force obtained in experiments without disturbance as the reference). It is clear from these results that under the proposed control, both the position errors and variances are much smaller than these under the benchmark controller. The force control performance in Fig. 4(b) shows that under the benchmark controller, the human have to respond to the disturbance with large applied force and delay in both the X- and Z-direction. Table II lists the RMS errors for the trajectory tracking and human-robot interaction forces under the benchmark and the proposed controllers for all subjects. The estimated disturbance force also follows the actual force closely.

We conducted additional experiments with lifting a weight

TABLE II ROOT MEAN SQUARE (RMS) ERRORS FOR CONTROL PERFORMANCE

ĺ	Control methods	Human f	Force (N)	End-effector position (mm)	
ı	Control methods	X-direction	Z-direction	X-direction	Z-direction
I	Benchmark control	$12.6 \pm 2.4$	$16.4 \pm 2.0$	$14.1 \pm 8.4$	$14.0 \pm 7.0$
ı	Proposed control	$6.6 \pm 1.6$	$6.4 \pm 1.0$	$8.6 \pm 3.4$	$8.5 \pm 4.0$

with  $f_l = 9.8$  N (i.e., 1 kg) with the same experimental protocol. Fig. 6(a) shows that with or without load  $f_l$ , human forces were similar to conduct the same movement task. To demonstrate the effectiveness of the proposed control, we compute the human efforts  $E_h$  defined by (3) during the aforementioned experiments. Fig. 6(b) shows the human effort comparison results. The plots include the statistical profiles of  $E_h$  by all subjects under the benchmark and the proposed controllers with disturbance, and also those under the benchmark controller without disturbance for comparison purpose. It is clearly shown by these results that under the proposed controller, the human effort under the disturbance

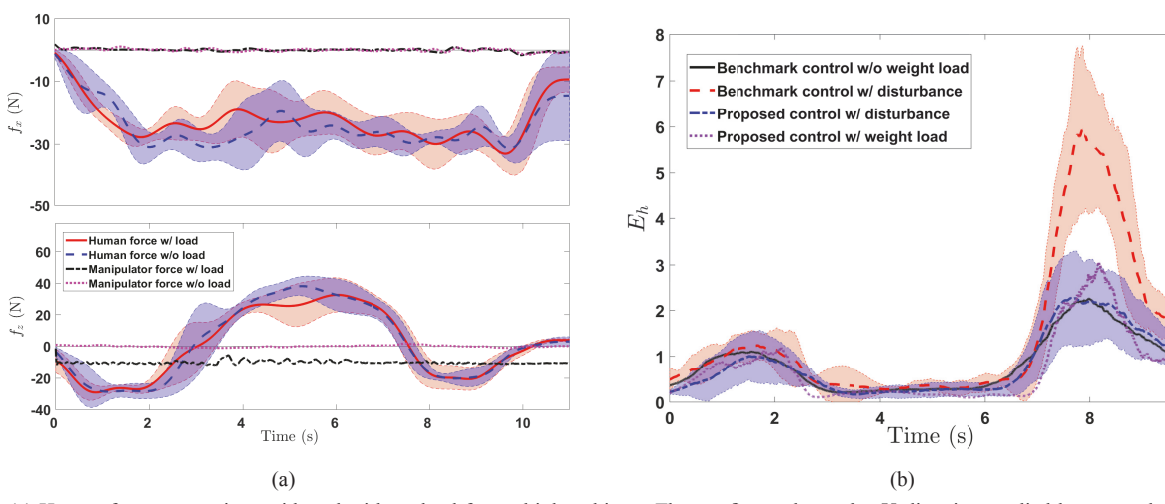


Fig. 6. (a) Human force comparison with and without load for multiple subjects. The top figure shows the X-direction applied human and robotic forces and the bottom for the Z-direction forces. The thick curves are the mean value profiles and the shaded areas show the one standard deviation around the mean values of all subject experiments. The same notation is used in all subjectes. (b) Human effort  $E_h$  comparisons under the benchmark and the proposed controllers. The results are obtained from all subject experiments.

(roughly from 6.5 to 10 s period) is much smaller than that under the benchmark controller.

#### V. CONCLUSION

We developed a muscle synergy-based force control of robotic manipulator for assist-as-needed physical humanrobot interactions. The muscle synergy model and the neural network approach were used to predict the muscle activation and then estimate human applied forces in human-robot interactions. A disturbance observer was designed to estimate the unknown external disturbance forces, and then an admittance control was applied to the manipulator to simultaneously follow human intention motion and to compensate for working load and undesired disturbances. The proposed force estimation did not need any EMG sensors, which was attractive in many physical human-robot interactions. This study mainly focuses on planar arm-manipulator motion tasks and some muscle properties are simplified. 3D motions. muscle fatigue and co-contraction in experiments are not considered which is one limitation of the proposed method.

### REFERENCES

- J. L. Emken, R. Benitez, and D. J. Reinkensmeyer, "Human-robot cooperative movement training: learning a novel sensory motor transformation during walking with robotic assistance-as-needed," J. Neuroeng. Rehabil., vol. 4, no. 1, p. 8, 2007.
- [2] A. Tran, "Robot confidence modeling and role change in physical human-robot collaboration," Ph.D. dissertation, Faculty Eng. Inform. Tech., Univ. Tech. Sydney, Sydney, Australia, 2019.
- [3] S. Chen, J. Yi, and T. Liu, "Strength capacity estimation of human upper limb in human-robot interactions with muscle synergy models," in *Proc. IEEE/ASME Int. Conf. Adv. Intelli. Mechatronics*, Auckland, New Zealand, 2018, pp. 1051–1056.
- [4] J. M. Inouye and F. J. Valero-Cuevas, "Muscle synergies heavily influence the neural control of arm endpoint stiffness and energy consumption," *PLoS Comput. Biol.*, vol. 12, no. 2, p. e1004737, 2016.
- [5] G. Torres-Oviedo and L. H. Ting, "Muscle synergies characterizing human postural responses," *J. Neurophysiol.*, vol. 98, no. 4, pp. 2144– 2156, 2007.
- [6] L. H. Ting and J. M. Macpherson, "A limited set of muscle synergies for force control during a postural task," *J. Neurophysiol.*, vol. 93, no. 1, pp. 609–613, 2005.

- [7] Y. Li and S. S. Ge, "Human-robot collaboration based on motion intention estimation," *IEEE/ASME Trans. Mechatronics*, vol. 19, no. 3, pp. 1007–1014, 2013.
- [8] S. S. Ge and C. Wang, "Adaptive neural control of uncertain mimo nonlinear systems," *IEEE Trans. Neural Networks*, vol. 15, no. 3, pp. 674–692, 2004.
- [9] J. L. McKay and L. H. Ting, "Functional muscle synergies constrain force production during postural tasks," *J. Biomech.*, vol. 41, no. 2, pp. 299–306, 2008.
- [10] F. Ficuciello, L. Villani, and B. Siciliano, "Variable impedance control of redundant manipulators for intuitive human–robot physical interaction," *IEEE Trans. Robotics*, vol. 31, no. 4, pp. 850–863, 2015.
- [11] S. Calinon, I. Sardellitti, and D. G. Caldwell, "Learning-based control strategy for safe human-robot interaction exploiting task and robot redundancies," in *Proc. IEEE/RSJ Int. Conf. Intell. Robot. Syst.*, Taipei, Taiwan, 2010, pp. 249–254.
- [12] E. Gribovskaya, A. Kheddar, and A. Billard, "Motion learning and adaptive impedance for robot control during physical interaction with humans," in *Proc. IEEE Int. Conf. Robot. Autom.*, Shanghai, China, 2011, pp. 4326–4332.
- [13] B. Yu, R. B. Gillespie, J. S. Freudenberg, and J. A. Cook, "Human control strategies in pursuit tracking with a disturbance input," in *Proc. IEEE Conf. Decision Control*, Los Angeles, CA, 2014, pp. 3795–3800.
- [14] D. G. Lloyd and T. F. Besier, "An EMG-driven musculoskeletal model to estimate muscle forces and knee joint moments in vivo," *J. Biomech.*, vol. 36, no. 6, pp. 765–776, 2003.
- [15] M. C. Tresch, V. C. Cheung, and A. d'Avella, "Matrix factorization algorithms for the identification of muscle synergies: evaluation on simulated and experimental data sets," *J. Neurophysiol.*, vol. 95, no. 4, pp. 2199–2212, 2006.
- [16] R. Sharif Razavian, N. Mehrabi, and J. McPhee, "A model-based approach to predict muscle synergies using optimization: application to feedback control," *Front. Comput. Neurosci.*, vol. 9, 2015, artical 121.
- [17] Y. Li and S. S. Ge, "Human–robot collaboration based on motion intention estimation," *IEEE/ASME Trans. Mechatronics*, vol. 19, no. 3, pp. 1007–1014, 2014.
- [18] M. W. Spong, S. Hutchinson, and M. Vidyasagar, *Robot modeling and control*. Wiley New York, 2006.
- [19] C. T. Landi, F. Ferraguti, L. Sabattini, C. Secchi, M. Bonfè, and C. Fantuzzi, "Variable admittance control preventing undesired oscillating behaviors in physical human-robot interaction," in *Proc. IEEE/RSJ Int. Conf. Intell. Robot. Syst.*, Vancouver, Canada, 2017, pp. 3611–3616.
- [20] K. P. Tee, R. Yan, and H. Li, "Adaptive admittance control of a robot manipulator under task space constraint," in *Proc. IEEE Int. Conf. Robot. Autom.*, Anchorage, AK, 2010, pp. 5181–5186.